PEER REVIEWED

Observation of Residual Stress and Fatigue Behavior of Structurally Integrated Thermally Sprayed Nickel Coatings

Gregory M. Smith[1,2] · John Saputo[1] · Vladimir Luzin[3,4] · Sanjay Sampath[1]

Abstract Fatigue behavior is strongly correlated with the residual stress state within thermal spray coatings, with neutral or compressive residual stresses being favorable for fatigue-sensitive applications. However, determination of the coating's residual stress state is predominately made prior to subjection of the coating to cyclic loading and does not give insight into possible changes to the residual stress state once in service. In this work, high-velocity, oxy-fuel nickel coatings were subjected to a partial fatigue loading regime, via both rotating bend fatigue and cantilever fatigue, targeting 99% of the total system fatigue life. Neutron diffraction was used to measure changes between the initial compressive residual stresses and after partial fatigue loading and was compared with the residual stress measurements made via beam curvature techniques during deposition. Results indicate that the fatigue credit typically associated with compressive residual stress coatings was partially dependent on the mode of loading and that there was a change in the residual stress magnitude due to changes during fatigue cycling. Additionally, metallographic assessment of the fracture surface was used to determine final fatigue failure within the substrate and crack propagation within the coating crossing through the substrate interface into the substrate.

Keywords fatigue · fracture · residual stress · structural integration

✉ Gregory M. Smith
gregory.m.smith@alumni.stonybrook.edu

1 Center for Thermal Spray Research, 130 Heavy Engineering Bldg., Stony Brook University, Stony Brook, NY 11794-2275, USA

2 Currently Located at Naval Research Laboratory, 4555 Overlook Ave SW, Washington, DC 20375, USA

3 Australian Nuclear Science and Technology Organization, Lucas Heights, NSW 2234, Australia

4 School of Engineering, The University of Newcastle, Callaghan, NSW 2308, Australia

Introduction

Residual stress measurement has been widely discussed in the context of production and fabrication of thermal spray coatings and has recognition as a crucial design element in coating application parameterization (Ref 1-4). Residual stress, or internal stress, refers to a stress distribution present within a structure in the absence of an applied external load (Ref 5). In thermal spray coatings, the confluence of impacting particles with differing degrees of peening and quenching forces, and the resulting formation of a range of microstructures makes determination and assessment of residual stress significantly more complex (Ref 2, 3, 6, 7).

Traditionally, microstructure formation due to rapid splat quenching and solidification and large thermal changes associated with deposition were drivers for residual stress change. However, the field has changed with the growth of low temperature, solid or semisolid-state processing, and high kinetic energy-based processes, such as high-velocity oxy-fuel (HVOF), high-velocity air–fuel (HVAF), warm spray (WS) and cold spray (CS) (Ref 8-15). The dominance of higher peening forces in these

applications has enabled consideration for structurally integrated coatings, which have been linked to hard chrome replacement efforts, structural repairs, hard-facing coatings and other fatigue-sensitive applications using both metals and cermet materials (Ref 16-21).

Of the range of techniques for measurement of residual stresses in thermal spray coatings, the beam curvature method and the neutron stress method represent two very distinct approaches. Beam curvature reflects a range of techniques for capturing the bilayer curvature effect of a two-layer, substrate/coating system, where deflection can be attributed to the global behavior of the system governed by an overall moment (Ref 1, 10, 22, 23). This provides for a measure of an overall system level, or global, stress state in the coating–substrate system, with the contribution of the entire coating assembly on the substrate being captured. In neutron-based assessment, lattice strain measurements on the atomic scale are used to calculate a more explicit, albeit highly localized, residual stress (Ref 24-27). Past work has shown relative agreement among both techniques for measurement of the residual stress states in thermal spray coatings for carbide and metal systems (Ref 28-32). With the strong link between residual stress, wear, corrosion and fatigue performance, determination of the residual stress state is critical, especially in structurally integrated coating systems.

The shift toward coatings being used in structurally integrated applications and now more readily (especially with emergence of CS) in metal repair applications, imparted residual stress are clearly important given the ability to tune these stresses with materials and process optimization. Peening-dominated processes tend toward higher compressive residual stress by nature of the solid-state particle impaction. This can reduce the apparent importance of the property from the perspective of a design engineer by potentially oversimplifying the need for process parameterization. Further complicating the application of residual stress is the question onto the static versus dynamic nature of the property once in service. Additionally, limited investigation into changes to the coating's residual stress state due to corrosion, fatigue or wear has occurred specifically for coating materials. During these modes of degradation and system damage, it would be expected that residual stress of the system could change.

In well-bonded metal and carbide systems formed by HVOF or CS processing, the question as to what happens to cracks that form within the coating can also arise in contemplation of how, or if, those cracks pose a risk to the attached substrate. Earlier work in coating system fatigue crack growth showed the possibility of crack deflection upon encountering a substrate interface or penetration into that substrate material (Ref 33, 34). Understanding the driving forces and susceptibility or the crack to 'jump'

across the substrate interface has serious operational and application implications. In a 'worst-case' scenario, a coating could act to inadvertently promote crack propagation across the substrate–coating interface with ultimate and pre-mature failure within the substrate.

In this work, the role of partial fatigue was investigated, with two different fatigue modes observed, namely cantilever bending and rotating bend fatigue (RBF). Measurement of residual stress was performed (both during coating formation and on deposited samples) and using the neutron measurement technique, a comparison was made between samples that underwent fatigue loading versus material remaining in its as-sprayed state. Finally, evaluation of the coating failure modes and crack pathways are performed via microscopy to identify and propose a route and mechanism for the system failure.

Experimental

Coatings were deposited on two different substrate geometries, namely cylindrical hourglass samples and flat beams, which are shown in Fig. 1. Cylindrical specimens were machined from cold-drawn 1018 steel ($E = 205$ GPa) and were heat-treated at 900 $^{\circ}$C for 2 h in vacuum to allow for stress relief and recrystallization of stresses induced by drawing and machining. Flat specimens were machined from 1008 mild-steel ($E = 200$ GPa) and went through a low-temperature stress relief treatment at 240 $^{\circ}$C for 2 h in vacuum.

Coating Deposition and In Situ Stress Measurement

HVOF deposition conditions are given in Table 1 and reflect a well-established parameter for a dense nickel coating (Ref 35, 36). Flat beams were held in a fixture allowing for concurrent measurement of in situ curvature, via laser displacement measurement. Additional samples
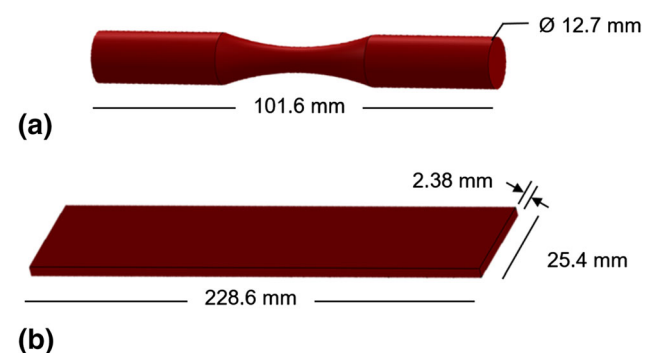

Fig. 1 Substrates used for fatigue testing, including cylindrical specimens (a) and flat beams (b), which were subsequently coated and evaluated

Table 1 Coating deposition conditions

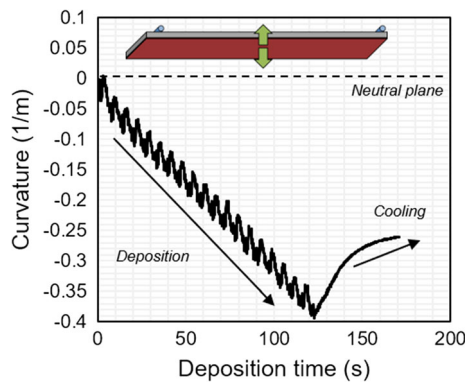| Powder/distribution	Torch	Barrel length, mm	Spray distance, mm	Raster speed, mm/s	Kerosene flow rate, l/h	Oxygen flow rate, l/m
Ni-914-3 (Praxair, Indianapolis, IN), $+10/-45$ μm	JP-5220 (Praxair/TAFA)	152.4	406	1000	22.7	943

Fig. 2 In situ beam curvature vs. time for the nickel coating deposition. Changes in curvature during deposition and subsequent relief during cooling left the beam in a permanently deflected state, noted by the difference of the final position and the neutral curvature level. Inset: Beam orientation showing the deflection during deposition and cooling

Fig. 3 Sample geometry and loading direction for the two different fatigue measurement techniques performed, including RBF (a) and cantilever bending (b)

were prepared and sectioned with a diamond wafer saw to final testing dimensions, per subsequent description. Coatings thickness was 365 ± 15 μm.

The beam curvature method for residual stress measurement has evolved over time from simple Almen strip evaluation, which is still used for characterization of residual stresses induced by grit blasting or shot peening processes. A simplified version of Stoney's formula can be used to measure evolving, thermal and residual stresses of a coating during the deposition processes (Ref 1, 6, 7). Real-time tracking and measurement of beam curvature are shown in Fig. 2 where successive passes can be seen as fluctuations in the evolving data (associated with localized beam deflection/movement as the spray torch moves across the surface) and which build, pass after pass, inducing successive changes to the beam curvature. This reaches a maximum, and then enters a cooling phase where the difference in the coating and substrate coefficient of thermal expansion drive thermal mismatch stresses. The final position of the curvature is then used to extrapolate the in-plane residual stress value. Additionally, by measuring coating strain during cool down, the elastic modulus of the coating can be calculated which has been widely discussed in the literature (Ref 4, 9, 22, 37).
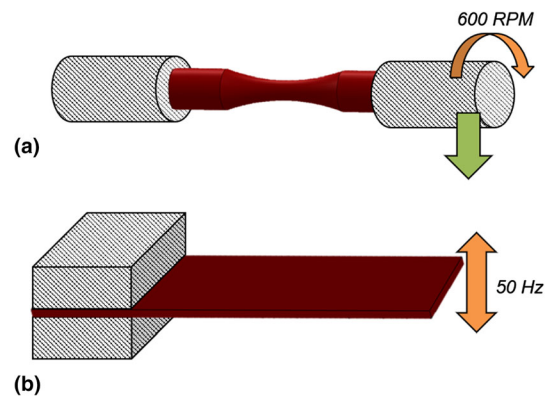
Fatigue Testing and Evaluation

Two different modes of cyclic fatigue loading were performed and are shown in Fig. 3. RBF is a well-established, and often preferred method of fatigue testing; however, for investigation of residual stresses via the neutron measurement, the sample geometry would conflate and make interpretation of the results difficult. To combat this, alternate test approaches were considered, which led to the cantilever bend method used here. This allowed a streamlined analysis, with residual stress measured during coating deposition via beam curvature, sectioning of the beam into two halves, and subsequent partial fatigue testing of the beams, for which a specific residual stress profile was known. Both partially fatigued (to 99% of the experimentally measured fatigue life, but with no visible coating/substrate damage apparent) and as-sprayed sample sections from near-fracture surface interface were then sent to the Australian OPAL research reactor facility (ANSTO) to undergo neutron diffraction investigations.

Cantilever fatigue testing was carried out using a VSS 40H cantilever bend fatigue machine (Fatigue Dynamics Inc., Dearborn, MI). The original sprayed beam was sectioned in half along the mid-span, resulting in two 114.3 mm × 25.4 mm segments. For testing, one segment was carefully positioned and held firm at one end of the

machine, while the other was attached to a crank wheel driven by an electric motor. The loading amplitude to which the cantilever was subjected changes throughout the rotational cycle, adjustable by the offset position of the eccentric crank angle. Due to limits on crack angle position the stress amplitude tended to be higher than in the RBF evaluation. The number of cycles to failure for the cylindrical bend fatigue was on the order of 10^4 to 10^5 cycles. Final failure typically occurred within the sample gauge near the fixed end.

For the cylindrical specimens, testing was carried out with an RBF-200 rotating bend fatigue machine (Fatigue Dynamics Inc., Dearborn, MI). Under these loading conditions, a constant load amplitude, with a non-uniform bending moment, was applied along the specimen length. The bending moment was applied via a sliding scale, using a known load at an adjustable distance. This gave a larger degree of flexibility in tailoring the stress amplitude with fatigue failures generated between 10^4 and 10^8 cycles. The hourglass shape of the cylindrical specimen concentrates the stress amplitude to a maximum along the narrow specimen gauge length, which was the location of failure in all the specimens. For both geometries, the nominal stress reported is based on the surface stress experienced by the uncoated specimen, normalized for the additional coating thickness.

Post-fatigue testing fracture surfaces were evaluated using scanning electron microscopy (SEM) (TM3000, Hitachi, Tarrytown, NY) in backscatter mode to investigate the location of the final fracture, associated cracking, delamination, fatigue striations, etc. No additional surface preparation was required for fracture specimens.

Neutron Stress Measurement

Determination of in-plane residual stress from measured strain profiles across the thickness of the coating and substrate was performed at ANSTO, using the KOWARI neutron strain scanner (Ref 24). While the basics of the experimental setup, measurement parameters for strain determination and analysis of experimental data within the predictive model approach for coating systems can be found elsewhere, additional details are provided here (Ref 26, 31, 32). Strain measurements were performed with a nominal gauge volume of $0.2 \times 0.2 \times 20$ mm^3, with the elongated gauge volume (oriented parallel to the in-plane direction and crack interface) used to maximize the diffraction signal while maintaining the required spatial resolution of 0.2 mm (Ref 26). Stresses were measured in the three principal directions, two in-plane and one normal to the coating surface, with 0.2 mm steps through the substrate thickness and 0.1 mm steps within the coating. Diffraction wavelengths, λ equal to 1.67 Å for the Fe (211)

and 1.50 Å for the Ni (311) reflections, respectively, provided the required 90-degree measurement geometries. The stress measurement accuracies achieved were $\sim$ 15 MPa for the steel substrates and $\sim$ 10 MPa for the Ni coatings.

A 'substrate-only' sample (with no coating) was also measured using the same measurement procedure in order to address possible pre-deposition stress within the substrate material (due to processing, e.g., cold rolling, grit blasting, etc.). However, after the stress relief heat treatment, such influences should be minimal. This profile was subtracted from the stress profiles of the coated samples so that the reported stress profiles are associated with the deposition process only.

Results

Generalized properties are shown in Table 2 for the nickel coating. Low porosity and moderate hardness are typical of HVOF sprayed metals (Ref 8, 35, 36). The elastic modulus of the coating is lower than for bulk nickel, which can be attributed to splat sliding and defects widely seen in thermal spray coatings, from brittle ceramics to metal coatings (Ref 37-40).

Residual stress differences between the beam curvature and the neutron profile measurements are apparent from Fig. 4 and Table 2. However, this is partially due to how the stresses were determined. Whereas the neutron measurement gives a location specific measurement of the residual stress profile in Fig. 4(b), the beam curvature presented in Fig. 4(a) shows a calculated linear distribution and does not account for any localized variations and nonlinearity. In general, localized stresses can vary, even within one particular coating, due to sensitivities to coating thickness, temperature, stress relaxation of localized defects, inhomogeneous defect structures, etc., which can fluctuate during deposition and over time and which in reality necessitate a large sampling of data. However, as an assessment tool both have significant benefits and careful use can give significant results and trends which are in general agreement between both methods.

The residual stress profile shown in Fig. 4(b) is notable for a few features, including a reduced compressive residual stress magnitude (as compared to the maximum compressive residual stress) near the free coating surface (+x axis). During deposition, incoming particles tend to peen the previously deposited layer, increasing the localized residual stress with successive deposition. However, near the surface of the coating, there are less successive passes of that peening action, and the very top layer undergoes no additional peening, which can be seen in the data presented. This may account for the reduced compressive residual stress in that location.

Table 2 General coating characteristics/properties

Porosity	Hardness HV0.3	Elastic modulus, GPa	Residual stress, MPa	
		Beam curvature	Beam curvature, Max	Neutron diffraction, Max
< 1%	365 ± 36	132 ± 13	−95 ± 10	−79.5 ± 15

Fig. 4 Residual stress distributions, as determined by in situ beam curvature (a) and neutron diffraction (b), showing nominally similar distributions, however with more features distinguishable via neutron diffraction due to the use of the much more sensitive technique
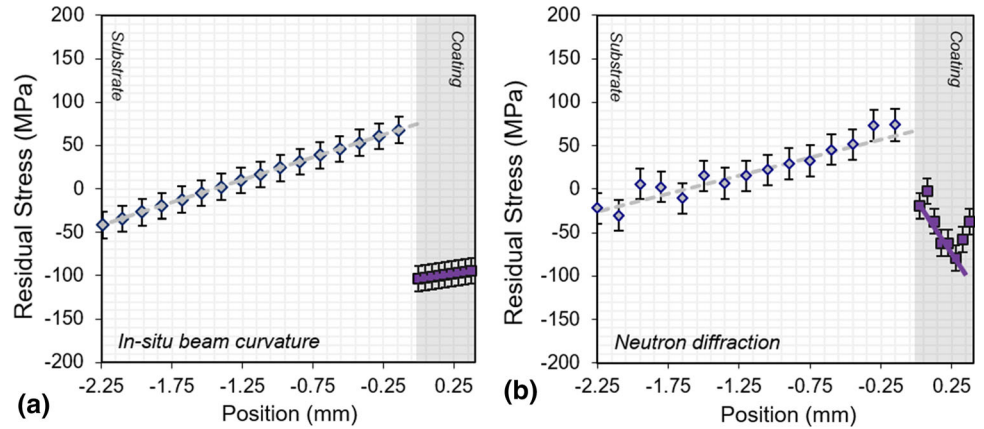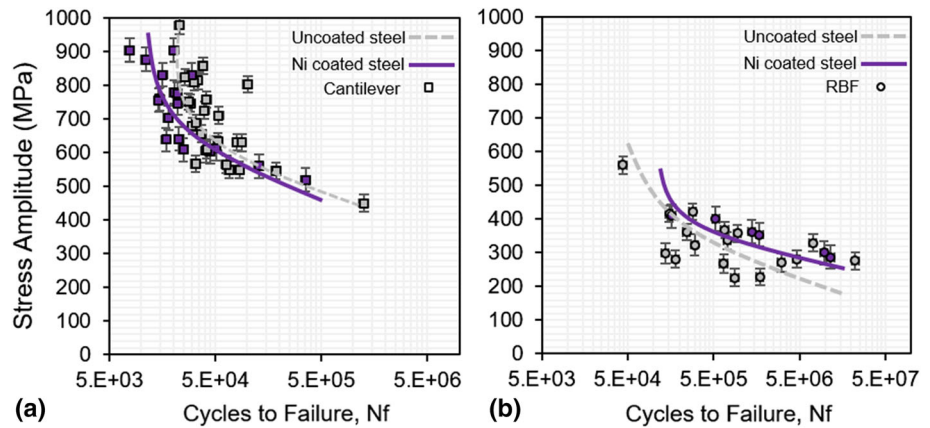

Fig. 5 Cantilever (a) and RBF (b) fatigue S–N results occupying two different regimes of the fatigue spectrum, due to loading and instrument constraints. For each set of data, 'best-fit' lines are overlaid. Error bars represent the standard deviation of three to five repeated tests

Data from both methods of fatigue assessment are presented in Fig. 5. Although the two modes segregate, there is a visible S–N curve for each, covering the range of fatigue results and trending toward the infinite fatigue life threshold. Under the RBF regime, there tended to be an increase in fatigue life (fatigue credit) in the coated samples, which has been presented widely in the literature for compressive residual stress coatings (and for general materials) (Ref 19, 20, 41). However, under the cantilever bend loading scenario, which due to limits of the machine tended to operate under higher loading conditions, the coated samples appear to show a decrease in performance versus the uncoated material (fatigue debit).

This fatigue debit may be the result of a combination of geometry factors, stress concentrations or other mechanisms at play. For example, in the cantilever geometry, only one side of the beam is coated, which creates a shift in the overall system stiffness and stress distribution.

Additionally, the planar shape and available edges of the beam and coating present additional free surfaces from which cracks can originate. The rotating bend sample, due to the uniformly distributed coating and balanced stress distribution, may alleviate some of these additional stress considerations. However, in real application, the flat cantilever beam may more closely replicate the free surface and radius of curvature for larger diameter components, and the single-sided coating may be a better approximation for how systems will behave where localized HVOF or CS repairs have been applied. This will be further examined in the discussion.

Partial Fatigue and Changes in Residual Stress

As introduced previously, the effect of partial fatigue on the residual stress state was of interest. During operation, coatings are subjected to a range of applied/operational

stresses and can experience unanticipated loads due to environmental effects, such as corrosion or abrasion. For coatings that are specifically targeted to have a compressive residual stress, often to combat fatigue, there tends to be an assumption that the intrinsic residual stress is static and will remain constant throughout the coating's operational life. The approach presented here reflects a method to measure the changes in residual stress after subjection of the coating to mechanical loading. Cantilever bend specimens were used due to their flat geometry being more favorable to eventual neutron stress measurement, which was used to characterize changes in the residual stress state after a known degree of partial fatigue.

Figure 6 shows the cantilever-only subset of the previously presented fatigue data, with an overlay of points, shown by open diamonds, from where partial fatigue tests were halted. These tests were stopped just prior to test failure and did not visually show any evidence of damage; however, these were all within the regime of which failure could be expected, and therefore likely had some accumulation of fatigue damage or crack growth. Determination of this 'stop' point was made based on targeting 99% of the logarithmic fatigue life, at a stress amplitude which gave approximately 20,000 oscillations.

After partial fatigue testing, 25.4 mm × 25.4 mm square sections were removed from the strain accumulation gauge section on both the as-sprayed and partially fatigued cantilever samples and were investigated by neutron diffraction. Resulting scans of both as-sprayed and partially fatigued samples are shown in Fig. 7 and indicate two subtle differences between the samples. The first, is the presence of an increased stress region in the partially fatigued specimen within the near-interface region of the substrate. This may be an artifact of the strain measurement, due to subtraction of the 'substrate-only' stress
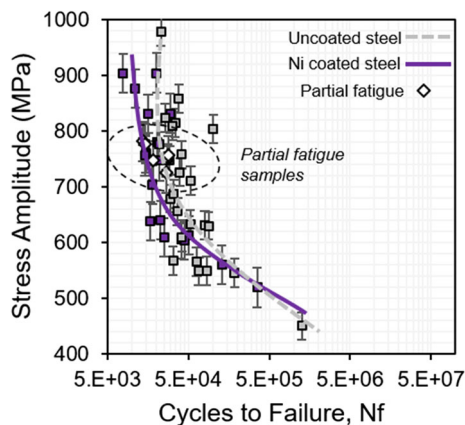
profile and possible statistical variations within the material. However, for this particular sample, the as-sprayed and partially fatigued specimens were complementary halves of the same beam and coated at the same time, so any 'substrate-only' influence would be expected to have been present within both. Additionally, this region also correlates well with the location of final failure in the substrate and will be elaborated upon further in the subsequent discussion. This lends more credence to this being a 'real' feature.

The other feature of note is the change in the magnitude of the residual stress, with an apparent increase in compressive residual stress within the coating after partial fatigue. The same general shape is present (slightly obscured by the overlaid trend line); however, the shift to higher residual stresses within the coating may indicate additional stress accumulation during the fatigue process. There are a few possible reasons for this uneven accumulation, which in part can be due to the effect of symmetric tension/compression cycles in an asymmetric system (coating only on one side). Due to the presence of microscopic defects, pores and micro-cracks within the coating, there is a differential ability of the coating to accommodate localized yielding, sliding, etc., while under tensile loading (Ref 38, 39). The same mechanism may be less pronounced in the coating while under compression loading, and so the symmetric oscillations between tension and compression cycling of the cantilever may lead to this asymmetric buildup.

Another reason for the uneven accumulation and asymmetric tension/compression distribution can be due to the uneven total applied stresses in the system after factoring in the residual stress profile. The total stress in the system can be simply expressed as the sum of the residual and applied stress profile, based on beam theory and bending of cantilever two-layer composites (Ref 42). The applied, residual and total stress profiles for the tensile loading portion of the cantilever cycle are shown in Fig. 8(a). The effect of the compressive residual stress (negative) reduces the magnitude of the total stress in the coating. Figure 8(b) shows the total stress profile for both tensile and compressive loading cycles, which because of the compressive residual stress within the coating, shifts the total stress further toward compression (or at least in the case of the tensile cycle, toward 'less tensile'). Additionally, the lower modulus of the coating with respect to the substrate results in a lower stress accumulation in the coating for the same applied strain.

The additional thickness of the coating, residual stress within the system, and nonlinearity of the coating causes a small shift in the neutral axis. This results in an increase in total tensile stress at the free (uncoated) substrate surface and a corresponding reduction in total tensile stress at the

Fig. 6 Cantilever fatigue S–N plot, with overlaid partially fatigued specimens, subjected to ∼ 99% of the estimated fatigue life cycles, with 'best-fit' lines overlaid. Error bars represent the standard deviation of three to five repeated tests

Fig. 7 Residual stress distributions, as determined by neutron diffraction, showing both the as-sprayed sample (a) and the partially fatigued sample (b), with an outline marking an increased stress region of interest. Specimens originated from the same coated beam
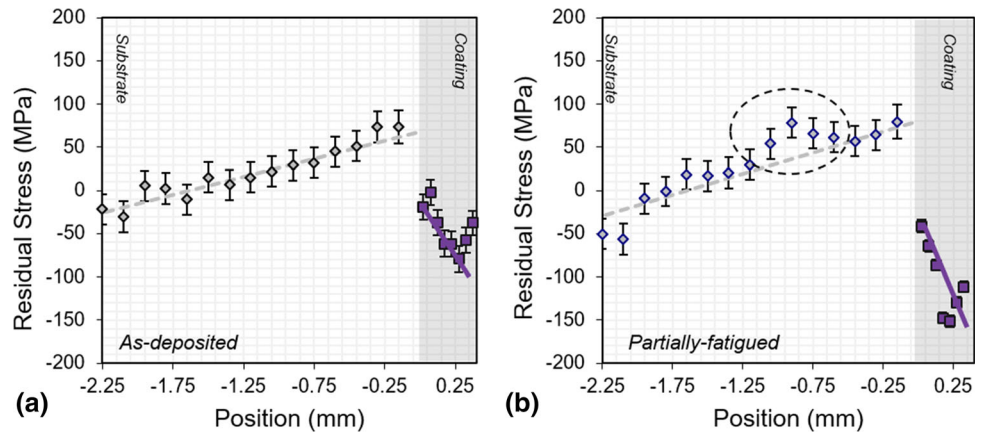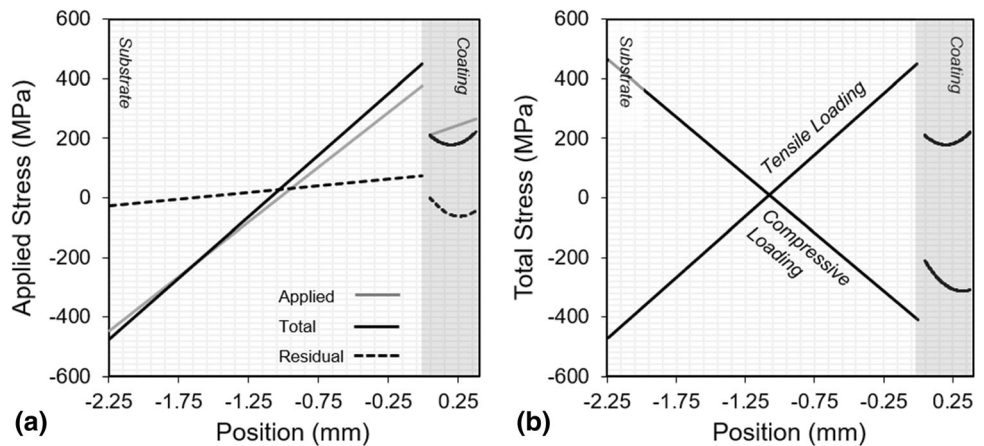

Fig. 8 Distribution of applied, total, and residual stresses under a tensile cycle of the cantilever bend fatigue loading (a) and distribution of total stress acting in both tension and compression cycles (b)

substrate–coating interface. The increase in total tensile stress may prompt an earlier onset of fatigue crack initiation, which also may partially explain the reduced fatigue life in the cantilever specimens versus RBF specimens. If both surfaces of the cantilever substrate (front/back) had been coated, this shift would not occur. Although the exact mechanism requires further investigation, microscopy of the fracture surfaces can shed some light onto the mechanisms at play and will be presented in the discussion. For this analysis, the coating free surface stress is used to calculate the stress amplitude and total stress. Because the coating is relatively thin (as compared to the substrate thickness) and with only moderate difference between coating/substrate elastic moduli, the difference between free surface and coating surface stress maximum is negligible.

Discussion

Analysis of the measured stress and determination of total applied stress can drive insight into the behavior and mechanisms as play during loading. After fatigue testing

and stress measurement, further investigation can be performed on the sample remains, specifically here on the fracture surfaces. Upon inspection of the fracture surfaces (obtained from samples tested to full failure), it is clear that the presence of the coating plays a role in shifting the final failure point within the substrate, as shown in Fig. 9. Additional evidence for this is shown in Fig. 7(b), where the dashed circle over the area of the residual stress profiles indicates the presence of an increased stress region, where a greater amount of tensile residual stress was measured. If one were to superimpose the fracture image over the residual stress position scale, it would be clear that this increased stress region aligns with the site of final failure in the coated sample. This region, notable as the site of final fracture, may be characterized by greater elastic deformation due to the large plastic zone around the propagating crack tip at this terminal location.

In the images without coating (uncoated steel substrate), the final fracture site is evenly distributed within the substrate, with the final failure and plastic deformation occurring at the neutral bend axis in the middle of the sample. However, in the case of the coated specimen, the changes in the distribution of the applied stress within the
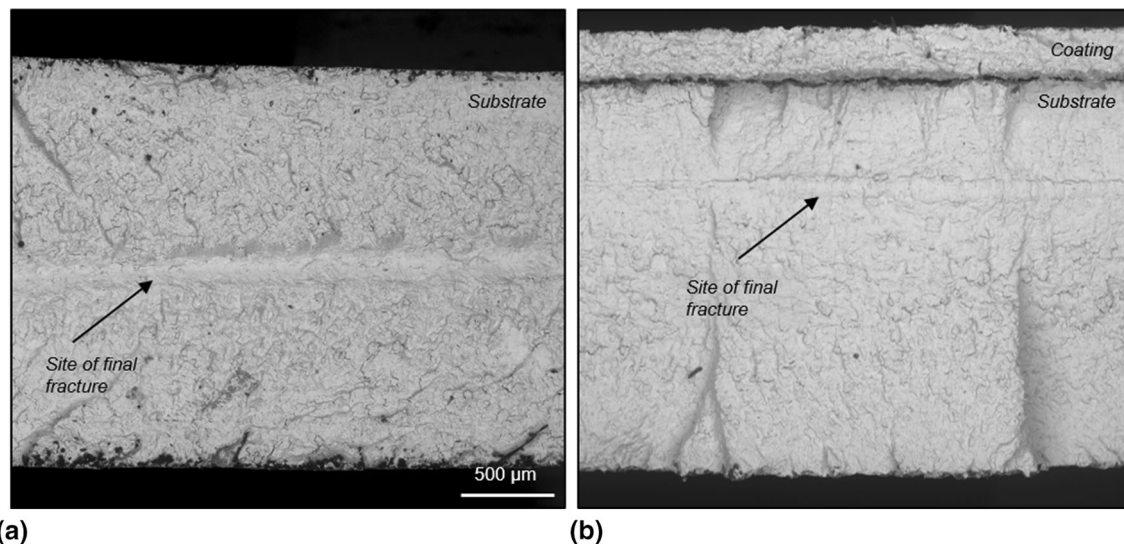
Fig. 9 Fracture surface of a cantilever fatigue sample, including both the uncoated cantilever beam (a) and the coated beam (b). Note the change in the position of the fatigue neutral bend axis

system, shifts the final fracture site toward the coating layer.

More detailed observation and location-based inspection can also be performed across the fracture surface, as shown in Fig. 10. In this set of fracture surfaces, the fatigue striations can be observed within the substrate (Fig. 10c and e) which reflect propagation of fatigue growth to the final failure site in Fig. 10(d). These striations are also present, albeit to a smaller degree, in Fig. 10(b), which indicate the coating is undergoing some degree of slower crack growth, relative to growth within the substrate. Also notable in Fig. 10 are the changes to the thickness of the coating layer (as compared to Fig. 9), which can slightly shift the position of this final failure site, due to the changes to the total stress within the system.

Fatigue striations were observed in periodic intervals on either side of the rupture point. Their widths can be used to infer nominal crack growth rates and make further interpretation regarding the mechanisms of failure. The crack growth can be empirically determined by measuring the mean fatigue striation widths as a function of position along the fracture surface of Fig. 10, with results shown in Fig. 11. Within the substrate the striations are smallest near the free substrate surface, which in conjunction with the high applied tensile stresses in this region suggest this as a site for crack initiation. Growing from the free substrate surface, the striations slowly increase in width until crossing the rupture point, after which fatigue striations are measurably larger, in the high residual tensile stress region within the substrate, below the substrate–coating interface.

Much smaller striations, < 0.5 μm, can be selectively seen in the coating and may indicate slower crack growth from within that region, which may be explained by a combination of the lower stiffness and existing compressive residual stresses. Failure in the coating is likely multimodal (with splat decohesion, localized fracture, disbandment, etc.) as striations are not uniformly visible (nor have uniform direction) and the defected microstructure of the HVOF coating presents numerous opportunities for more complex failure modes (Ref 43, 44). The striations below the substrate–coating interface begin disproportionately small and then rapidly increase as they approach the rupture point suggesting the crack growth rapidly increased due to the high residual tensile stresses in that region.

Based on prior evaluation, the adhesion and cohesion strength of similar nickel coatings is high (Ref 28, 36, 45). In addition to the prior description regarding the role of residual stress resulting in asymmetric loading and the shift in the neutral plane, the presence of similar coatings has also been shown to enable partial load-sharing in mechanical systems which lend themselves toward structurally integrated application (Ref 35, 36, 45). In such application, the role of the coating as an integrated component of the system requires additional considerations with regards to fatigue-sensitive applications.

Based on the availability of free energy in the coating–substrate system, and from prior observation, the assumption thus far has been that crack initiation will begin on both free surfaces and then grow inward. In past work, cracks have been noted as growing through the coating and then propagating across the coating–substrate interface, at least in instances where the coating is well-bonded (Ref 20, 21, 36, 46, 47). Both Vackel, et al. and Varis, et al., support final fracture occurring within the substrate, after progression through the system (Ref 20, 21). It has also been shown in past work, e.g., Vackel, et al., that crack
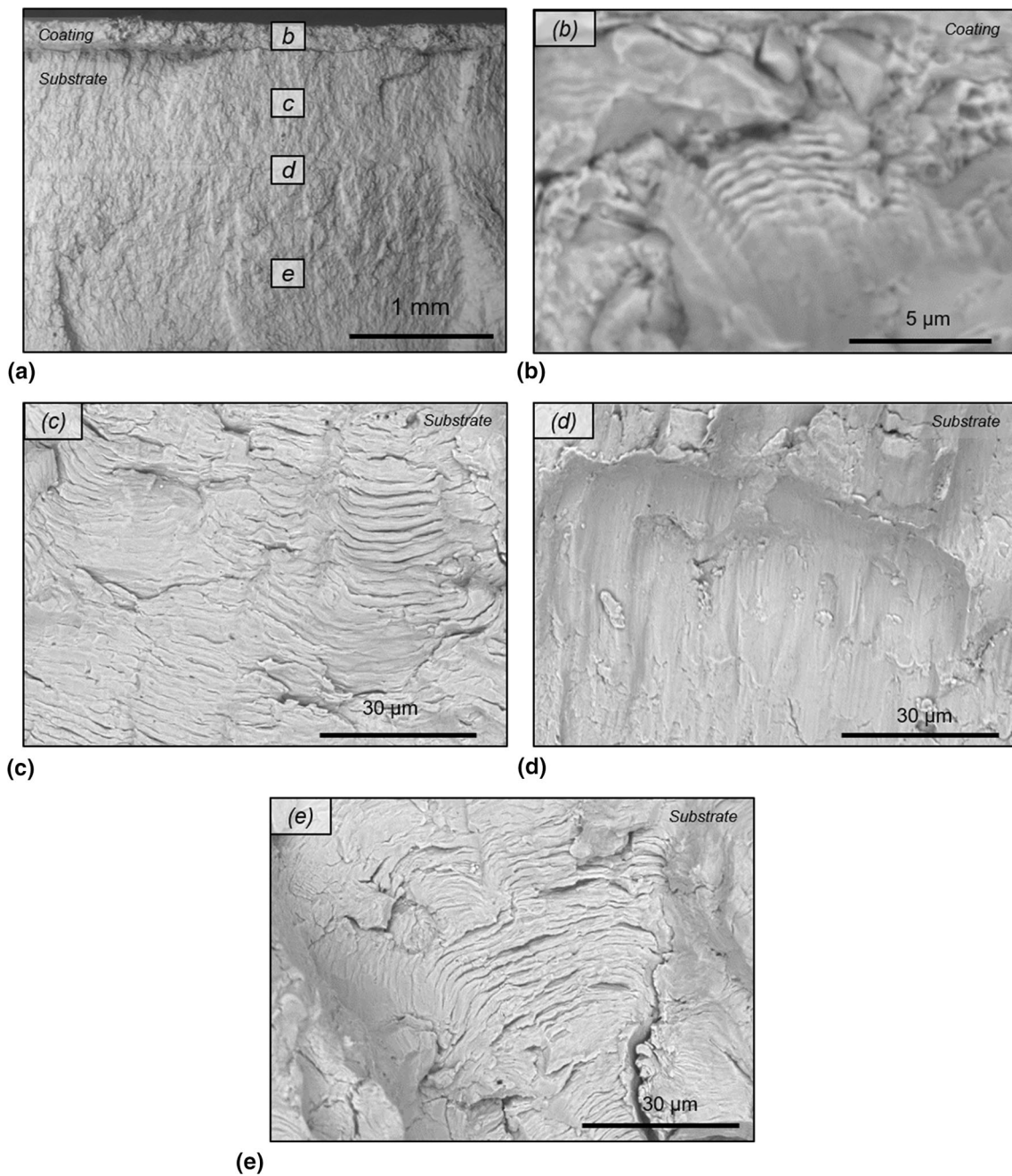
Fig. 10 Fracture surface of cantilever fatigue sample (a), showing higher resolution images of highlighted regions within the coating (b) (note scale difference), within the near-interface region of the substrate (c) and the lower portion of the substrate (e), showing progression of the crack front through the metal, and then the failure location at the mid-line (d)

propagation can also deflect at the interface, due to a breakdown of the mechanical cohesion in poorly bonded or weakly cohesive coatings (Ref 20).

The tendency for a crack to originate at the free surface or within the coating and to subsequently penetrate across the interface and into the substrate reinforces earlier assessment (Ref 33, 34). Work by Suresh and Sugimura, et al., showed that with sufficient energy and for a sufficiently bonded interface, a crack will cross through and continue propagation within the substrate, following the gradient from the harder coating layer or material and penetrating the softer substrate material (Ref 33, 34). In a weakly bonded system, a propagating crack from the coating would potentially bifurcate and delaminate at the coating–substrate interface as a mode of energy dissipation, rather than continue to grow through the substrate. Or, due to differences in moduli between coating and substrate, a localized disbondment can occur, creating an energy

concentration to drive further crack growth in each direction. This balance between delamination and crack propagation has been tangentially observed and discussed but has significant implications in fatigue behavior.

A proposed pathway for crack growth in this scenario is illustrated in Fig. 12. This varies notably from the propagation in cylindrical specimens, operated either under cyclical/RBF or axial loading (Ref 20, 21). In this progression, the crack would likely start at both free surfaces

Fig. 11 Spacing between fatigue crack striations, with a notable increase within the tensile residual stress area between the failure zone and the coating–substrate interface

and progress inward, albeit at a slower rate through the coating. The evidence of fatigue striations growing toward the final fracture site within the substrate indicate the pathway a crack would take across the interface where it will ultimately link up with the complimentary crack in the sub-interface region (Ref 48). The smaller striation size observed in the coating, combined with the reduced stress amplitude driven by stiffness and the compressive residual stress, lead to a lower probability of fatigue crack growth and indicates that cohesive failures are more likely at lower stresses than expected in bulk materials.

To directly observe this behavior, one sample was carefully monitored during testing and halted immediately prior to full failure (defined by separation of the two sections). This would not be reflective of the partially fatigued samples, for which test was halted prior to any observable crack growth. A polished (0.05% colloidal Al_2O_3) cross section was taken from the sample fracture surface and is shown in Fig. 13. Unexpectedly for high adhesion HVOF coatings, significant delamination is present at the coating–substrate interface, which based on literature may be more prevalent under bending modes that traditional RBF loading (Ref 49, 50). This is still in alignment with the hypothesized crack pathway from Fig. 12, with the crack growth continuing into the substrate from beneath the
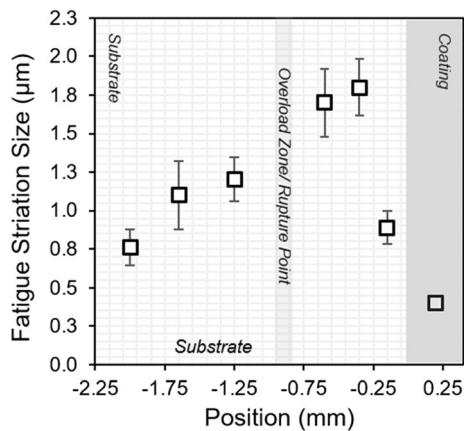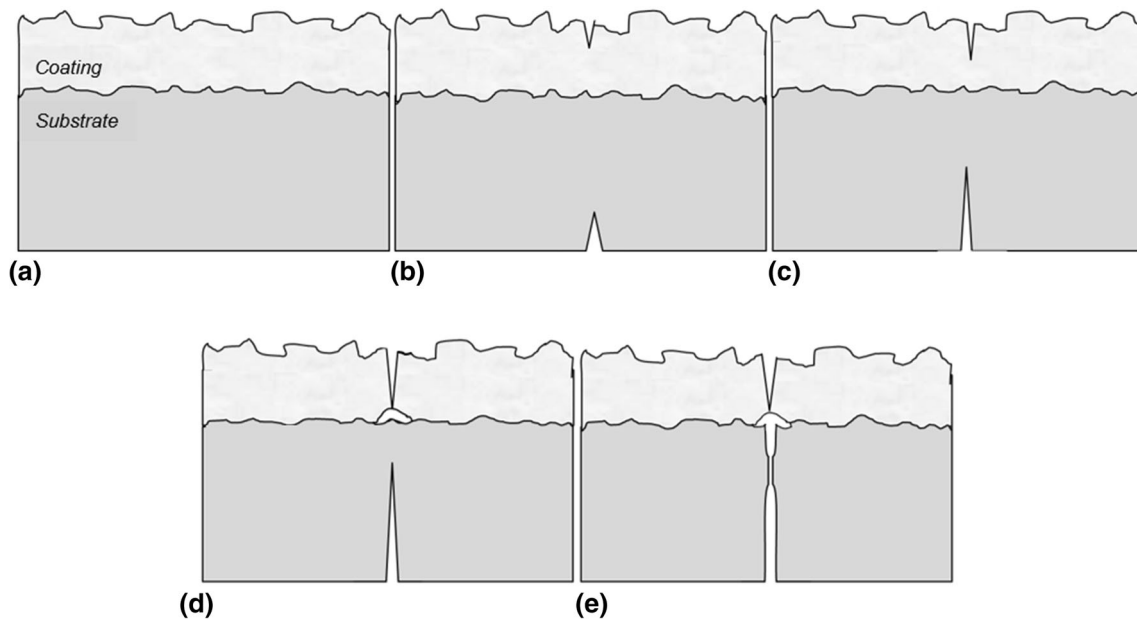

Fig. 12 Hypothesized crack propagation pathway, with crack initiation in both the coating and substrate and growing (a-c) and then reaching and coalescing within the steel substrate (d-e), below the coating/substrate interface
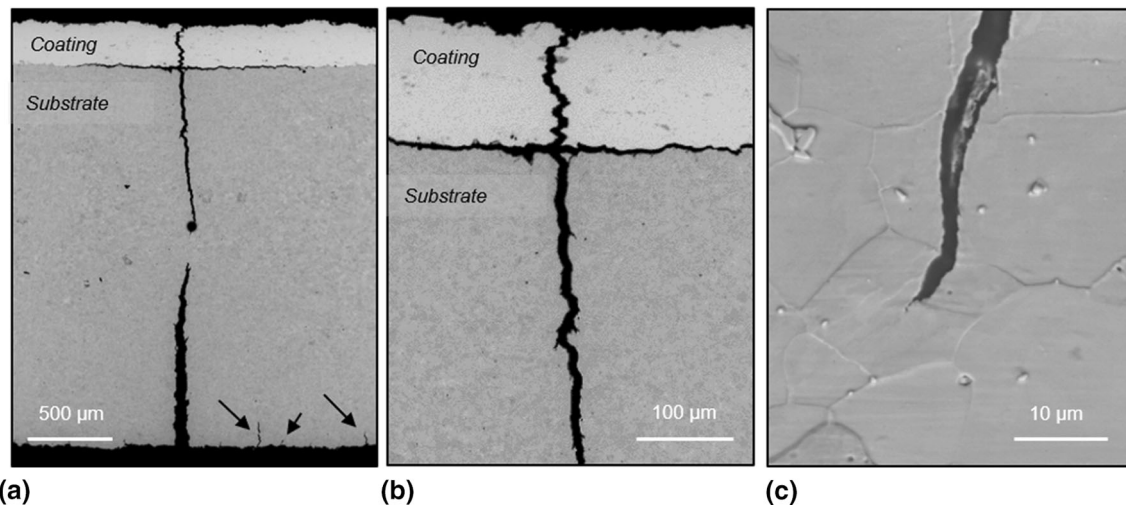
Fig. 13 Polished cross section of coated specimen after fatigue testing at low magnification (a), high magnification (b), and higher yet, showing intra-granular propagation of the crack within the substrate (c). Several additional cracks, indicated by arrows, can be observed on the non-coated side of the steel substrate under low magnification (a). Note—The sample, as shown here, would be considered as in a "failed" state, and not reflective of the partially fatigued condition

coating, where a localized disbondment/loss of adhesion has occurred.

Conclusion

In the work presented, two techniques for the measurement of residual stress were used before and after subjection of coated specimens to a partial loading regime via cantilever bend fatigue. The indication from the results points to the idea that the distribution of the residual stresses within a system can be influenced by the application of additional stresses into the system (e.g., by mechanical loading). Due to the geometry and test configuration used here, this had the effect of increasing the compressive residual stress within the coating surface during cantilever fatigue loading.

This effect is likely influenced heavily by the modality of the fatigue loading and of the substrate/system geometry. As shown in the results, the mode of fatigue loading (cantilever versus RBF) effects the previously established idea of a fatigue credit/debit due to the asymmetry and distribution of stresses in a specimen with only a single-side coated. It would therefore also make sense that the buildup or change in residual stress, as well as the final mode of failure due to the loading regime, would also be subject to change with sample geometry, etc.

For full establishment of mechanisms, additional fatigue loading scenarios should be contemplated. For flat panels/ beams such as were used here, comparing results with beams that were coated on both sides would be of additional interest to gauge how they differ. Typically, the fatigue behavior of uncoated surfaces is well-established, whereas the exposed, coated surface represents the surface of interest. Further investigation into damage propagation and crack translation across the coating/substrate interface warrants similar diverse investigation, especially with varying coating and substrate material hardness, as that potential source of failure has strong implications in many current and future structurally integrated coating application.

References

1. T.W. Clyne and S.C. Gill, Residual Stresses in Thermal Spray Coatings and Their Effect on Interfacial Adhesion: A Review of Recent Work, *J. Therm. Spray Technol.*, 1996, **5**(4), p 401-418
2. M. Gui, R. Eybel, B. Asselin, S. Radhakrishnan, and J. Cerps, Influence of Processing Parameters on Residual Stress of High Velocity Oxy-Fuel Thermally Sprayed WC-Co-Cr, *Coating*, 2012, **21**(10), p 2090-2098
3. S. Sampath, X.Y. Jiang, J. Matejicek, L. Prchlik, A. Kulkarni, and A. Vaidya, Role of Thermal Spray Processing Method on the Microstructure, Residual Stress and Properties of Coatings: An Integrated Study for Ni–5 wt%Al Bond Coats, *Mater. Sci. Eng. A*, 2004, **364**(1), p 216-231
4. S. Sampath, V. Srinivasan, A. Valarezo, A. Vaidya, and T. Streibl, Sensing, Control, and in Situ Measurement of Coating Properties: An Integrated Approach Toward Establishing Process-Property Correlations, *J. Therm. Spray Technol.*, 2009, **18**(2), p 243-255
5. J. Schijve, Ed., *Residual Stress, Fatigue of Structures and Materialsed*, Springer, Dordrecht, 2009, p 89-104
6. S. Kuroda, T. Dendo, and S. Kitahara, Quenching Stress in Plasma Sprayed Coatings and Its Correlation with the Deposit Microstructure, *J. Therm. Spray Technol.*, 1995, **4**(1), p 75-84

7. S. Kuroda, Y. Tashiro, H. Yumoto, S. Taira, H. Fukanuma, and S. Tobe, Peening Action and Residual Stresses in High-Velocity Oxygen Fuel Thermal Spraying of 316l Stainless Steel, *J. Therm. Spray Technol.*, 2001, **10**(2), p 367-374

8. T.S. Sidhu, S. Prakash, and R.D. Agrawal, State of the Art of HVOF Coating Investigations—A Review, *Mar. Technol. Soc. J.*, 2005, **39**(2), p 53-64

9. T. Suhonen, T. Varis, S. Dosta, M. Torrell, and J.M. Guilemany, Residual Stress Development in Cold Sprayed Al, Cu and Ti Coatings, *Acta Mater.*, 2013, **61**(17), p 6329-6337

10. A. Valarezo, W.B. Choi, W. Chi, A. Gouldstone, and S. Sampath, Process Control and Characterization of NiCr Coatings by HVOF-DJ2700 System: A Process Map Approach, *J. Therm. Spray Technol.*, 2010, **19**(5), p 852-865

11. D.E. Wolfe, T.J. Eden, J.K. Potter, and A.P. Jaroh, Investigation and Characterization of Cr3C2-Based Wear-Resistant Coatings Applied by the Cold Spray Process, *J. Therm. Spray Technol.*, 2006, **15**(3), p 400-412

12. J. Kawakita, H. Katanoda, M. Watanabe, K. Yokoyama, and S. Kuroda, Warm Spraying: An Improved Spray Process to Deposit Novel Coatings, *Surf. Coat. Technol.*, 2008, **202**(18), p 4369-4373

13. R.K. Kumar, M. Kamaraj, S. Seetharamu, T. Pramod, and P. Sampathkumaran, Effect of Spray Particle Velocity on Cavitation Erosion Resistance Characteristics of HVOF and HVAF Processed 86WC-10Co4Cr Hydro Turbine Coatings, *J. Therm. Spray Technol.*, 2016, **25**(6), p 1217-1230

14. J.A. Browning, Viewing the Future of High-Velocity Oxyfuel (HVOF) and High-Velocity Air Fuel (HVAF) Thermal Spraying, *J. Therm. Spray Technol.*, 1999, **8**(3), p 351-356

15. S. Kuroda, M. Watanabe, K. Kim, and H. Katanoda, Current Status and Future Prospects of Warm Spray Technology, *J. Therm. Spray Technol.*, 2011, **20**(4), p 653-676

16. J.M. Guilemany, N. Espallargas, P.H. Suegama, and A.V. Benedetti, Comparative Study of Cr3C2–NiCr Coatings Obtained by HVOF and Hard Chromium Coatings, *Corr. Sci.*, 2006, **48**(10), p 2998-3013

17. A. Ibrahim and C.C. Berndt, Fatigue and Deformation of Hvof Sprayed WC–Co Coatings and Hard Chrome Plating, *Mater. Sci. Eng. A*, 2007, **456**(1), p 114-119

18. B.D. Sartwell, K. Legg, P. Bretz, E., Status of HCAT/JP-PP Program on Replacement of Hard Chrome Plating with HVOF Thermal Spray Coatings on Landing Gear, *Proc. of AESF Aero. Plat. Met. Fin. For.*, 2000, p 131-139

19. A. Vackel, G. Dwivedi, and S. Sampath, Structurally Integrated, Damage-Tolerant, Thermal Spray Coatings, *JOM*, 2015, **67**(7), p 1540-1553

20. A. Vackel and S. Sampath, Fatigue Behavior of Thermal Sprayed WC-CoCr- Steel Systems: Role of Process and Deposition Parameters, *Surf. Coat. Technol.*, 2017, **315**, p 408-416

21. T. Varis, T. Suhonen, O. Calonius, J. Čuban, and M. Pietola, Optimization of HVOF Cr3C2NiCr Coating for Increased Fatigue Performance, *Surf. Coat. Technol.*, 2016, **305**, p 123-131

22. J. Matejicek and S. Sampath, In Situ Measurement of Residual Stresses and Elastic Moduli in Thermal Sprayed Coatings: Part 1: Apparatus and Analysis, *Acta Mater.*, 2003, **51**(3), p 863-872

23. J. Matejicek, S. Sampath, D. Gilmore, and R. Neiser, In Situ Measurement of Residual Stresses and Elastic Moduli in Thermal Sprayed Coatings: Part 2: Processing Effects on Properties of Mo Coatings, *Acta Mater.*, 2003, **51**(3), p 873-885

24. O. Kirstein, V. Luzin, and U. Garbe, The Strain-Scanning Diffractometer Kowari, *Neutron News*, 2009, **20**(4), p 34-36

25. A.J. Allen, M.T. Hutchings, C.G. Windsor, and C. Andreani, Neutron Diffraction Methods for the Study of Residual Stress Fields, *Adv. Phys.*, 1985, **34**(4), p 445-473

26. V. Luzin, K. Spencer, M. Zhang, N. Matthews, J. Davis, and M. Saleh, *Residual Stresses in Cold Spray Coatings, Cold-Spray Coatings: Recent Trends and Future Perspectives*, P. Cavaliere, Ed., Springer, Berlin, 2018, p 451-480

27. J. Gibmeier, H.C. Back, M. Mutter, F. Vollert, J. Rebelo-Kormeier, R. Mücke, and R. Vaßen, Study of Stability of Microstructure and Residual Strain After Thermal Loading of Plasma Sprayed YSZ by Through Surface Neutron, *Scanning*, 2018, **551**, p 69-78

28. G.M. Smith and S. Sampath, Sustainability of Metal Structures Via Spray-Clad Remanufacturing, *JOM*, 2018, **70**(4), p 512-520

29. W.B. Choi, L. Li, V. Luzin, R. Neiser, T. Gnäeupel-Herold, H.J. Prask, S. Sampath, and A. Gouldstone, Integrated Characterization of Cold Sprayed Aluminum Coatings, *Acta Mater.*, 2007, **55**(3), p 857-866

30. J. Matějíček, S. Sampath, T. Gnäeupel-Herold, and H.J. Prask, Residual Stress in Sprayed Ni + 5%Al Coatings Determined by Neutron Diffraction, *Appl. Phys. A*, 2002, **74**(1), p 1692-1694

31. V. Luzin, K. Spencer, and M.X. Zhang, Residual Stress and Thermo-Mechanical Properties of Cold Spray Metal Coatings, *Acta Mater.*, 2011, **59**(3), p 1259-1270

32. V. Luzin, A. Vackel, A. Valarezo, and S. Sampath, Neutron Through-Thickness Stress Measurements in Coatings with High Spatial Resolution, *Mater. Sci. Forum*, 2017, **905**, p 165-173

33. Y. Sugimura, P.G. Lim, C.F. Shih, and S. Suresh, Fracture Normal to a Bimaterial Interface: Effects of Plasticity on Crack-Tip Shielding and Amplification, *Acta Mater.*, 1995, **43**(3), p 1157-1169

34. S. Suresh, *Fatigue of Materials*, 2nd ed., Cambridge University Press, Cambridge, 1998

35. A. Vackel, T. Nakamura, and S. Sampath, Mechanical Behavior of Spray-Coated Metallic Laminates, *J. Therm. Spray Technol.*, 2016, **25**(5), p 1009-1019

36. X. Luo, G.M. Smith, and S. Sampath, On the Interplay Between Adhesion Strength and Tensile Properties of Thermal Spray Coated Laminates—Part I: High Velocity Thermal Spray Coatings, *J. Therm. Spray Technol.*, 2018, **27**(3), p 296-307

37. A. Valarezo and S. Sampath, An Integrated Assessment of Process-Microstructure-Property Relationships for Thermal-Sprayed NiCr Coatings, *J. Therm. Spray Technol.*, 2011, **20**(6), p 1244-1258

38. T. Gnäeupel-Herold, H.J. Prask, J. Barker, F.S. Biancaniello, R.D. Jiggetts, and J. Matejicek, Microstructure, Mechanical Properties, and Adhesion in IN625 Air Plasma Sprayed Coatings, *Mater. Sci. Eng. A*, 2006, **421**(1), p 77-85

39. Z. Wang, A. Kulkarni, S. Deshpande, T. Nakamura, and H. Herman, Effects of Pores and Interfaces on Effective Properties of Plasma Sprayed Zirconia Coatings, *Acta Mater.*, 2003, **51**(18), p 5319-5334

40. G.M. Smith, A. Smith, and S. Sampath, Fracture Toughness of Thermal Spray Ceramics: Measurement Techniques and Processing Dependence, *J. Therm. Spray Technol.*, 2018, **27**(7), p 1076-1089

41. G.M. Smith and S. Sampath, Sustainability of Metal Structures Via Spray-Clad Remanufacturing, *JOM*, 2018, **70**, p 512-520

42. J.M. Gere and S. Timoshenko, *Mechanics of Materials*, PWS Publishing Company, New Orleans, 1997

43. O. Kovářík, P. Haušild, J. Medřický, L. Tomek, J. Siegl, R. Mušálek, N. Curry, and S. Björklund, Fatigue Crack Growth in Bodies with Thermally Sprayed, *Coating*, 2016, **25**(1), p 311-320

44. O. Kovarik, A. Materna, J. Siegl, J. Cizek, and J. Klecka, Fatigue Crack Growth in Plasma-Sprayed Refractory Materials, *J. Therm. Spray Technol.*, 2019, **28**(1), p 87-97

45. X. Luo, G.M. Smith, and S. Sampath, On the Interplay between Adhesion Strength and Tensile Properties of Thermal Spray

Coated Laminates—Part II: Low-Velocity Thermal Spray Coatings, *J. Therm. Spray Technol.*, 2018, **27**(3), p 308-318

46. G.M. Smith, O. Higgins, and S. Sampath, In-Situ Observation of Strain and Cracking in Coated Laminates by Digital Image Correlation, *Surf. Coat. Technol.*, 2017, **328**, p 211-218

47. M.A.M. Halmi, M.A. Harimon, L.M. Tobi, and M.F. Mahmod, Fatigue Performance of Thermal Spray Coatings on Carbon Steel: A Review, *Int. J. Mech. Eng. Technol.*, 2019, **10**(3), p 1285-1300

48. N.W. Sachs, Understanding the Surface Features of Fatigue Fractures: How They Describe the Failure Cause and the Failure History, *J. Fail. Anal. Prev.*, 2005, **5**(2), p 11-15

49. A. Silvello, P. Cavaliere, A. Rizzo, D. Valerini, S. Dosta Parras, and I. Garcia Cano, Fatigue Bending Behavior of Cold-Sprayed Nickel-Based Superalloy Coatings, *J. Therm. Spray Technol.*, 2019, **28**(5), p 930-938

50. L. Janka, J. Norpoth, R. Trache, S. Thiele, and L.-M. Berger, HVOF- and HVAF-Sprayed Cr3C2-NiCr Coatings Deposited from Feedstock Powders of Spherical Morphology: Microstructure Formation and High-Stress Abrasive Wear Resistance up to 800 & #xB0;C, *J. Therm. Spray Technol.*, 2017, **26**(7), p 1720-1731